

RESEARCH

Open Access



Thermal behavior and cyclic fatigue resistance of three contemporary NiTi heat-treated single-file systems: metallurgical study

Loai Alsofi^{1*}, Mazen Al-Marshadi^{1,2}, Tariq AbuHaimed³, Mey Al-Habib¹, Rajab Saif¹, Sarah Bukhari¹ and Mohammed Howait¹

Abstract

Background This study aims to determine phase transformation temperatures of EndoSequence Reciprocating System (ESR), Wave One Gold (WOG), and Reciproc Blue (RB) via differential scanning calorimetry (DSC). Further, to evaluate the cyclic fatigue behaviors by applying static (SF) and dynamic fatigue (DF) tests.

Methods All files' systems were evaluated using DSC (Netzch 200 F3, Germany) with scans ranging from 80°C to -80°C to compare phase transformation. Twenty files from each file system ($n = 20$) were tested by cyclic fatigue in SF ($n = 10$) and in DF ($n = 10$) and the number of cycles to failure (NCF) was calculated for all groups. The files were rotated in a clockwise motion in a metal tube at 350rpm. The NCF was calculated by multiplying the time until fracture in minutes by speed (350 rpm). The NCF was analyzed statistically using a One-Way Analysis of Variance (ANOVA) to determine if there were significant differences among the experimental groups.

Results All files exhibited a single peak in the cooling curve marking martensitic transformation with RB showing martensitic transformation start temperature at around 37°C. ESR and WOG exhibited single endothermic peaks marking austenitic transformation. RB exhibited two endothermic peaks marking R-phase and austenitic transformations. In cyclic fatigue testing, WOG presented the lowest NCF in DF testing compared to ESR and RB ($p < .05$) with a nonsignificant difference between the latter two. In the SF, ESR showed a statistically significant larger NCF compared to RB, which also showed statistically significant larger NCF compared to WOG ($p < .05$).

Conclusions RB shows martensite transformation start temperature close to body temperature. RB and ESR show improved cyclic fatigue resistance compared to WOG in the SF mode. In the DF mode, WOG showed the lowest cyclic fatigue resistance.

Keywords Nickel-Titanium alloy, Differential scanning calorimetry, Phase transformation, Cyclic fatigue

*Correspondence:

Loai Alsofi
lalsofi@kau.edu.sa

¹ Department of Endodontics, Faculty of Dentistry, King Abdulaziz University, P.O. Box 80209, Jeddah 21589, Saudi Arabia

² King Faisal Hospital, Ministry of Health, Makkah, Saudi Arabia

³ Department of Restorative Dentistry, Faculty of Dentistry, King Abdulaziz University, Jeddah, Saudi Arabia

Introduction

The manufacturing of nickel-titanium (NiTi) endodontic instruments with improved properties such as super flexibility [1], shape memory [2], and low modulus of elasticity, led to reduced instrumentation errors during root canal treatment [3–5]. Single-file reciprocating nickel-titanium systems were introduced for root



© The Author(s) 2025. **Open Access** This article is licensed under a Creative Commons Attribution-NonCommercial-NoDerivatives 4.0 International License, which permits any non-commercial use, sharing, distribution and reproduction in any medium or format, as long as you give appropriate credit to the original author(s) and the source, provide a link to the Creative Commons licence, and indicate if you modified the licensed material. You do not have permission under this licence to share adapted material derived from this article or parts of it. The images or other third party material in this article are included in the article's Creative Commons licence, unless indicated otherwise in a credit line to the material. If material is not included in the article's Creative Commons licence and your intended use is not permitted by statutory regulation or exceeds the permitted use, you will need to obtain permission directly from the copyright holder. To view a copy of this licence, visit <http://creativecommons.org/licenses/by-nc-nd/4.0/>.

canal instrumentation by YarEd, 2008 [6]. Reciprocating files engage and cut dentine when rotating in counterclockwise motion (CCW) and disengage in clockwise (CW) reverse motion. Reciprocating motion appears to decrease the risk of file separation caused by cyclic fatigue failure compared to continuous rotation [7, 8].

One of the most important advancements in producing engine-driven files is represented by the development of thermomechanical treatment of the conventional nickel-titanium alloy. Lately, special heating–cooling treatments have resulted in the formation of a titanium oxide layer on the surface of the instrument. VDW Germany (VDW, Munich, Germany) introduced Reciproc Blue (RB) files, an evolution of Reciproc M wire [9]. RB is thermally treated to improve the mechanical properties of the file, such as flexibility, cutting efficiency, and fatigue resistance [9, 10]. RB has an S-shaped cross-section, two cutting edges, and a noncutting tip, and it is manufactured by proprietary “blue heat treatment” [11]. De-Deus et al. studied the effect of Blue thermomechanical treatment on fatigue resistance and flexibility [10, 12]. The study concluded that thermally blue-treated files showed improved flexibility and enhanced fatigue resistance compared with the original Reciproc files [10].

Wave One Gold (WOG) (Dentsply Sirona, Charlotte, NC, USA) is another reciprocating single file system that is manufactured with a parallelogram cross-section and has an off-centered design with two cutting edges. Gold-wire technology is performed by heating and then slowly cooling the file after machining. The thermal treatment results in a special surface color corresponding to the titanium oxide layer [13]. The file features a single cutting edge that contacts the canal wall during movement, alternating with its noncentral cross-section. This design helps reduce both the attachment and the screwing effect of the file on the canal wall [14]. Both manufacturers claim that the heat treatment of both WOG and RB has been proven to be superior to Wove One and Reciproc in curved canals due to their superior flexibility and cyclic fatigue resistance [9, 10, 15].

EndoSequence Reciprocating System (ESR) (Brasseler, Savannah, GA USA) has a reverse cutting flute design, progressive rectangular cross-section, and heat treatment to increase its resistance to fracture [10, 16]. The manufacturer claims that the ESR file system preserves more coronal tooth structure than WOG because of its taper. ESR Files are electropolished to remove the surface imperfections naturally present in NiTi. This process yields a cleaner, safer, and more efficient file. Previous reports show that electropolishing of NiTi instruments improves cyclic corrosion behavior with varying effects on cyclic fatigue resistance [17, 18].

These files’ super-flexibility and shape memory effects are related to martensitic transformation. At room temperature, nickel-titanium alloy consists of an austenite phase while at lower temperatures nickel-titanium consists of a martensitic phase [19]. A decrease in the temperature can induce phase transformation from austenite to martensite (martensite or reverse transformation) and conversely increase in temperature causes forward transformation from martensite to austenite. This transformation can also be induced by stress [20]. The reverse martensitic transformation is the reason for the super flexibility of nickel titanium instruments which facilitate the preparation of curved canals [21]. Furthermore, the rhombohedral (R phase) precedes austenitic or martensitic transformation under certain conditions. Phase transformation behavior is influenced by heat treatment and manufacturing processes [22, 23].

Differential scanning calorimetry (DSC) indicates which of the three phases (martensitic, R-phase, or austenitic) will be present at a given temperature. Structural transformations in the NiTi alloys are revealed as endothermic peaks on the heating DSC curve which represents the austenite transformation temperatures. Structural transformations in the NiTi alloys are revealed as exothermic peaks on the cooling DSC curve which represents the martensitic transformation temperatures. Information is obtained about the temperature ranges and enthalpy changes for the phase transformations [24, 25].

Instrument separation during canal preparation remains a major concern and it can be caused by either torsional or cyclic fatigue [26–29]. Several studies have reported that cyclic fatigue is the most common cause of failure in curved canals [30]. Cyclic fatigue is attributable to repetitive tensile and compression stresses in the instrument as it rotates in a curved canal [29]. Increasing resistance to cyclic fatigue has been the focus of the advancement of NiTi rotary instrument technology, and improvements in the manufacturing process are among the strategies proposed to increase these NiTi instruments’ mechanical properties. The shift to reciprocating rotary instruments and the use of heat-treated wires have been shown to increase NiTi instruments’ cyclic fatigue resistance [9].

The three NiTi mentioned previously are all used in reciprocation motion and are all heat-treated. In this study, we aim to characterize phase transformation temperatures of RB, WOG, and ESR and to compare the cyclic fatigue resistance of these files in both static (SF) and dynamic (DF) modes. Fractured instruments were examined using SEM. The null hypothesis was that there would be no difference between the three systems

regarding their phase transformation and cyclic fatigue resistance (SF and DF).

Materials and methods

This study was approved by the Research Ethics Committee of the Faculty of Dentistry, King Abdulaziz University, proposal no. 195–12–20. Three reciprocating NiTi instruments were used in this study: ESR size # 25 with variable taper by Brasseler, WOG size #25/0.07 by Dentsply, and RB size # 25/0.08 by VDW. From each NiTi system, five instruments were used ($n=5$) for phase transformation analysis. The sample size was based on previous reports [31].

The working part of each file starting from the tip was cut into 10 mm long samples weighing approximately 10–15 mg each. All files' systems were evaluated using DSC (Netzsch 200 F3, Germany) with scans ranging from 80°C to –80°C to compare phase transformation and thermal behavior. Each sample was placed in an aluminum pan. The pan was sealed and placed in the measuring chamber of DSC which was equipped with a controlled cooling device. Nitrogen was used as a purge gas. The temperature was increased from room temperature to 80°C at a rate of 10°C / min and then cooled to –80°C at a rate of –10°C /min to obtain the cooling curve to evaluate transformation temperature and phase transformation. The temperature was subsequently increased back to 80°C at a rate of 10°C to obtain the heating curve to evaluate phase transformation and phase thermal behavior.

The transformation temperatures obtained from the DSC curves for each specimen include the martensitic transformation start temperature (M_s) and finish temperature (M_f), the austenitic transformation start temperature (A_s) and finish temperature (A_f), as well as the R-phase transformation start temperature (R_s) and finish temperature (R_f). The interpretation of the DSC curves was based on methodologies and findings reported in previous studies [22, 32, 33].

Moreover, individual or combined peak areas were calculated from the DSC curve. The heating and cooling rate was carried out 5 times per file. The tangent lines, where the DSC curve deviates from and returns to the baselines, were denoted as starting and finishing temperatures. The transformation temperatures were calculated from the intersection between the extrapolation of the baseline and the maximum gradient line of the DSC curve.

A total of 60 instruments, 20 instruments from each group ($n=20$), were subjected to a universal testing machine (MultiTest 2.5-i, Mecmesin, Slinfold, UK). The sample size was selected based on previous reports [34, 35]. A sample size calculation was conducted using G-Power (v. 3.1) and showed that a sample size of $n=20$

per group was adequate to obtain a type I error rate of 5% and a power of 80%. Contra-angle handpiece with 1:16 reduction (Sirona, 64,625 Bensheim, Germany) and Electric endodontic motor (Setelec I- Endo Dual, Acteon, France) were used. Using a particular setup, the endodontic motor's handpiece was attached to the universal testing machine's moving arm in the vertical direction. In the lower part of the universal testing machine, an artificial canal made of stainless steel was attached to the chuck vice. The vice was attached to a two-dimensional horizontal micro-positional stage to accurately align the artificial canal with its descending instrument. According to the Pruett method, the artificial canal's angle was 60 degrees with a radius of 5 mm [36]. The artificial canal was designed to accommodate the rotary instruments tested with a tip size of 25 and 8% taper. Each artificial canal depth was luster-milled to the instrument's maximum diameter of +0.2 mm, allowing the instrument to rotate freely inside the canal. The artificial canal was covered with glass to prevent the fractured part of the instrument from sliding out before further investigation. Following Nguyen et al., a drop of synthetic oil (WD-40 Company, Milton Keynes, England) was used while testing the rotary instrument to reduce the friction between the instrument and the artificial canal, which prevents the temperature from increasing [37].

In the SF mode, ten instruments from each group were rotating freely in a CW direction within the stainless-steel artificial canal, and the maximum curvature was located 3 mm from the instrument's tip. In the DF mode, the instruments were moving vertically to simulate the clinical pecking motion. A continuous axial oscillating motion was applied at 1 (Hz) cycle per second. Each instrument cycled 3 mm above and 3 mm below the starting point, resulting in a net oscillation movement of 6 mm. Custom-made software (Mecmesin, Slinfold, UK) was used to control the axial motion.

The time to fracture in seconds was calculated using a video recording with a high-resolution camera (D3200; Nikon, Tokyo, Japan). A digital stopwatch was started when the instrument began to rotate until the first sign of fracture. The number of cycles to failure (NCF) was calculated by multiplying the time until fracture in minutes by speed (350 rpm).

Two fractured segments per file system were selected randomly for fractographic analysis under scanning electron microscope (SEM) (AURA 100 Scanning Electron Microscope, Seron, Korea). To determine the characteristics of the fractured segments, a single evaluator examined the fractured segments under 300× and 500× magnification to confirm that instrument separation was attributable to cyclic fatigue. During fractographic analysis, the evaluator identified crack origin and

propagation, as well as striations and dimples that caused the instrument to fail.

Statistical analysis

Prior to analysis, the data for the NCF was transformed using the Box-Cox method to approximate normality and meet the assumptions of ANOVA. The NCF was analyzed statistically using a One-Way Analysis of Variance (ANOVA) to determine if there were significant differences among the experimental groups. Following a significant ANOVA result ($p < 0.05$), pairwise comparisons were performed using Tukey’s Honest Significant Difference (HSD) test to identify specific group differences at a 95% confidence level. Statistical analyses were conducted using SPSS (v. 11.0, SPSS Inc., Chicago, IL, USA) and Python for transformation and validation.

Results

All files showed thermal transformation and displayed reproducible DSC scans but with different phase transformations at varying transformation temperatures. As shown in Fig. 1, the typical DSC curve of the RB file exhibited two endothermic peaks on the heating curve. The first peak coincides with the transformation from martensite to R-phase and the second peak coincides

with the transformation from R-phase to austenite. The cooling curve shows a single peak, which marks the transformation from austenite to martensite. Figures 2 and 3 show the typical DSC curves for ESR and WOG, respectively. Both figures show two heating curves and one cooling curve. Each heating curve shows a single peak, which marks the transformation from martensite to austenite. The cooling curves show a single peak, which marks the transformation from austenite to martensite. Comparison between the heating curves shows that the austenitic transformation peak was identified at higher temperatures for WOG compared to RB and ESR. The thermal peaks for RB were nearly equal to 23.7°C for R-phase transformation and around 35°C for austenitic transformation. The thermal peak for ESR was nearly equal to 29.19°C for austenitic transformation. For WOG, the thermal peak for austenitic transformation was around 45.73°C. In reverse transformation, the peak martensitic transformation temperature was around 28.61°C for RB, 21.45°C for ESR, and 41.47°C for WOG. Tables 1 and 2 summarize phase transformation temperatures and average enthalpy for each transformation for all three files.

In forward transformation, all phase transformation temperatures were higher for WOG (A_s : 32.82 ± 0.31

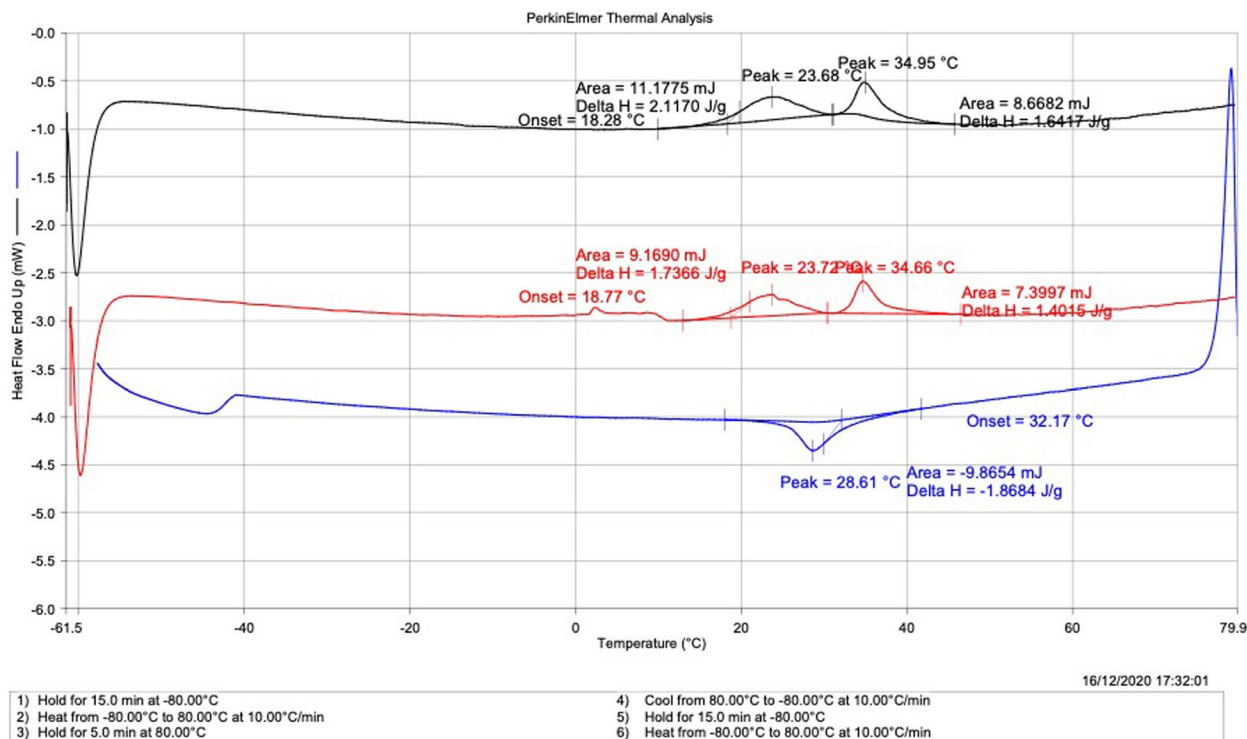


Fig. 1 DSC curves of RB during Cooling and Heating. The images show two heating (endothermic) curves (black and red) and one cooling curve (exothermic) (blue). The heating curves show two peaks, one coincides with the transformation from martensite to R-phase and the second peak coincides with the transformation from R-phase to austenite. The peak on the cooling curve marks the transformation from austenite to martensite

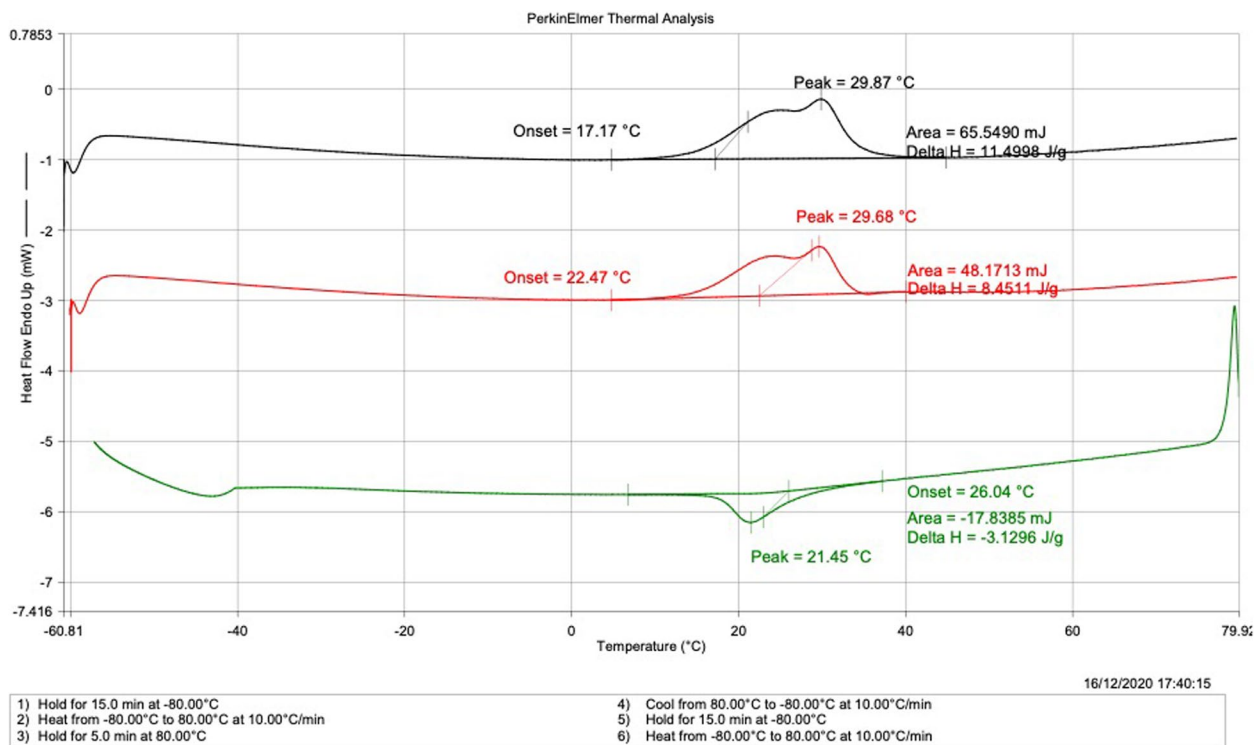


Fig. 2 DSC curve of ESR during heating and cooling. The images show two heating curves (endothermic) (black and red) and one cooling curve (exothermic) (green). The cooling curve shows a single peak that coincides with the transformation from austenite to martensite. The peak on the heating curve marks the transformation from martensite to austenite

°C, A_f : 61.8 ± 0.5 °C) than for ESR (A_s : 9.5 ± 0.32 °C, A_f : 36.62 ± 0.87 °C) and RB (A_s : 31.32 ± 0.92 °C, A_f : 43.62 ± 0.47 °C) but ΔH values were higher for ESR (11.7416 ± 0.2644 H ($J g^{-1}$)) than RB (1.5594 ± 0.195 ($J g^{-1}$)) and WOG (2.59316 ± 0.3532 ($J g^{-1}$)).

Twenty instruments from each system were subjected to a cyclic fatigue test with 10 in statements ($n=10$) subjected to SF and 10 in statements ($n=10$) subjected to DF. In SF, ESR had a mean of 3701 ± 629.07 NCF which was statistically significant ($p < 0.05$) compared to RB with 2860.55 ± 572.39 NCF. In the same mode (SF), WOG had 976.85 ± 215.13 NCF which was statistically significant ($p < 0.05$) from both ESR (3701 ± 629.07 NCF) and RB (2860.55 ± 572.39 NCF). In DF, WOG showed 1748.25 ± 254.63 NCF which was statistically significant ($p < 0.05$) compared to both ESR (6495 ± 1366.63 NCF) and RB (6662.95 ± 1410.20 NCF). Overall, all systems examined in this experiment exhibited a statistically significant larger NCF in the DF mode than in the SF mode ($p < 0.05$) (Table 3).

The fractographic analysis demonstrated the common features of cyclic fatigue failure, as shown in Figs. 4 and 5. Fractographic analysis revealed larger areas of striations in the DF mode groups compared to the SF mode groups.

Discussion

The results and data analysis of the phase transformation, thermal behavior, and cyclic fatigue resistance revealed significant differences among the 3 file systems. Thus, the null hypothesis was rejected. Multiple factors affect the phase transformation behaviors of NiTi endodontic instruments. These factors could be intrinsic to the metal or extrinsic such as temperature, stress, manufacturing process, and heat treatment [38–40]. The transformation temperature is one of the most important factors that affect the mechanical properties of nickel-titanium alloy. A complete understanding of the phase transformation influenced by temperature changes is crucial for the efficient and safe use of NiTi rotary instruments. Miyai et al. and Brantley et al. concluded that differences in the transformation temperatures of nickel-titanium instruments cause differences in the mechanical properties and behavior of these instruments under different conditions [25, 32]. The results of the present study showed that M_s and M_f points of WOG were higher than those for RB and ESR. This could indicate decreased flexibility of WOG files as its martensitic starting temperature is very high compared to body temperature.

RB shows two endothermic peaks on the heating curve indicating that the transformation of the alloy

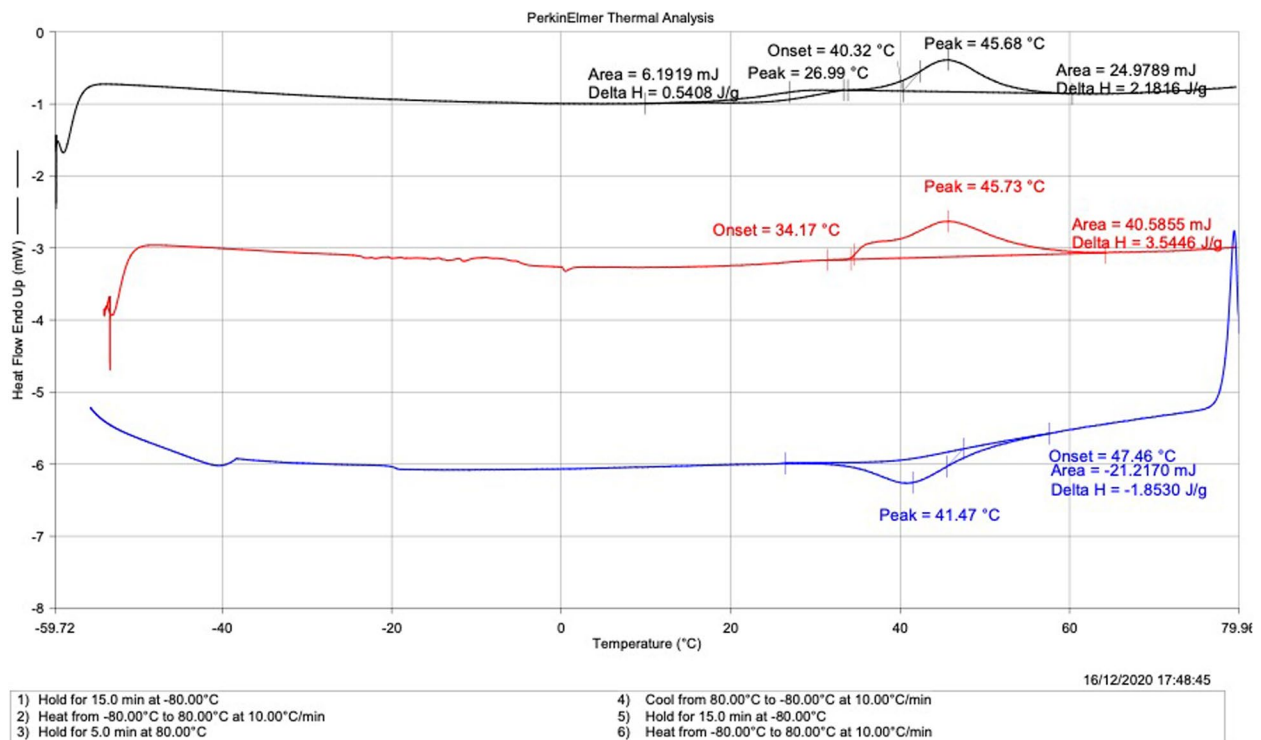


Fig. 3 DSC curve of WOG during heating and cooling. The images show two heating curves (endothermic) (black and red) and one cooling curve (exothermic) (blue). The cooling curve shows a single peak that coincides with the transformation from austenite to martensite. The peak on the heating curve marks the transformation from martensite to austenite

Table 1 Phase transformation temperatures (° C) and associated energy enthalpy H (J g⁻¹) for RB, ESR, and WOG during heating

ΔH (J g ⁻¹)	A_f (° C)	A_s (° C)	ΔH (J g ⁻¹)	R_f (° C)	R_s (° C)	Files
11.7416 ± 0.2644	36.62 ± 0.87	9.5 ± 0.32	-	-	-	ESR
2.59316 ± 0.3532	61.8 ± 0.5	32.82 ± 0.31	-	-	-	WOG
1.5594 ± 0.195	43.62 ± 0.47	31.32 ± 0.92	2.58338 ± 0.3639	30.26 ± 0.43	15.84 ± 0.78	RB

(Mean ± standard deviation)

Table 2 Phase transformation temperatures (° C) and associated energy enthalpy H (J g⁻¹) for RB, ESR, and WOG during cooling

ΔH (J g ⁻¹)	M_f (° C)	M_s (° C)	Files
-3.16628 ± 0.0805	12.57 ± 0.59	33.27 ± 0.91	ESR
-1.81946 ± 0.0642	30.96 ± 0.79	55.2 ± 0.49	WOG
-1.86056 ± 0.453	22.06 ± 1.18	37.35 ± 0.76	RB

(Mean ± standard deviation)

passes through the intermediate R-phase that shows complex transformation behavior tracing back to the manufacturing process. R-phase transformation has been reported in other rotary systems such as Hyflex EDM, ProTaper Gold files, and Vortex Blue files [41, 42]. The intermediate R-phase may exist in Nickel-rich

files, this phase may exist between austenite and martensite transformations [43, 44]. The R-phase is characterized by superior fatigue resistance [45] and it is favored by the presence of Ti₃Ni₄ particles [41]. According to a study by Hieway et al., an R-phase peak was detected during the martensitic transformation of vortex blue, and it was found that the A_f temperature of vortex blue is 38°C [41, 46].

RB file shows martensitic transformation starting temperature close to body temperature. This could indicate greater flexibility and resistance to fracture during clinical use. The calculated associated energy (ΔH) was lower for RB and WOG than ESR. RB file shows A_f temperatures higher than working temperature, which may indicate that this file has stable martensite and R-phase

Table 3 Mean ± standard deviation of NCF to failure of three reciprocating files RB, ESR, and WOG in the SF mode and the DF mode

Group	Number	Minimum NCF	Maximum NCF	Mean ± SD NCF	Statistical significance
ESR (SF)	10	2898	5075	3701 ± 629.07 ^a	^a <i>p</i> < 0.05
ESR (DF)	10	5033	9513	6495 ± 1366.63	^c <i>p</i> < 0.05
WOG (SF)	10	717.5	1431.5	976.85 ± 215.13 ^a	^a <i>p</i> < 0.05
WOG (DF)	10	1515.5	2285.5	1748.25 ± 254.63	^b <i>p</i> < 0.05 ^c <i>p</i> < 0.05
RB (SF)	10	1753.5	3888.5	2860.55 ± 572.39 ^a	^a <i>p</i> < 0.05
RB (DF)	10	4581.5	8809.95	6662.95 ± 1410.20	^c <i>p</i> < 0.05

^a indicates statistical significance between systems in the SF and

^b indicates statistical significance between systems in the DF

^c indicates statistical significance for each system between SF and DF modes

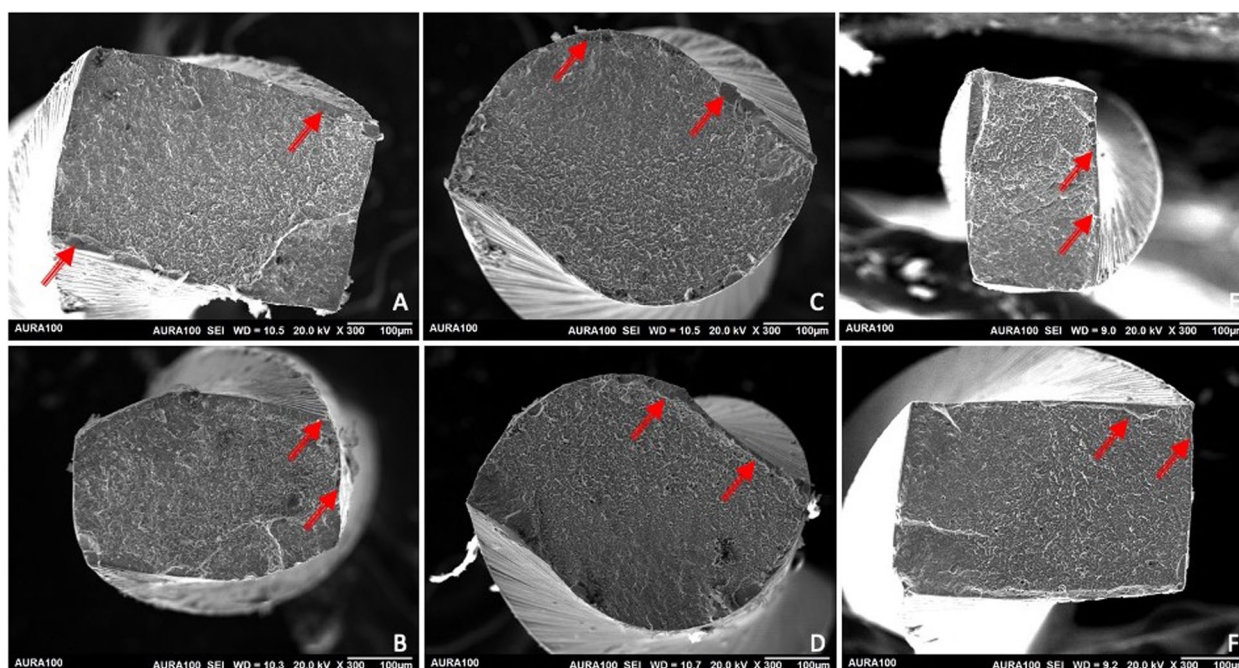


Fig. 4 Fractographic analysis images of ESR, RB, and WOG taken at 300X magnification using SEM. **A, C,** and **E** show fractured segments of ESR, RB, and WOG, respectively, after cyclic fatigue in static mode. **B, D,** and **F** show fractured segments of ESR, RB, and WOG, respectively, after fatigue in dynamic mode. Red arrows show multiple areas of fatigue crack initiation

while being used, which will favor super elasticity [47]. The increased austenitic transformation temperatures of NiTi files could be due to heat treatment during manufacturing [48].

In this study, we used CW continuous rotation rather than reciprocation motion in cyclic fatigue testing to standardize the kinematics between the files and to avoid any friction caused by rotating the file in its cutting direction. Various cyclic fatigue test devices can be utilized with either SF or DF test models. In SF models, the instrument rotates at a fixed length within the artificial canal without any axial movement [49]. The DF test

model was also used with an axial movement of 3 mm, as it is considered to more accurately replicate clinical conditions compared to SF models [35, 50]. The results of SF and DF resistance indicate that WOG has the fewest NCF compared to other brands. These results were consistent with previous reports that WOG has fewer cycles to failure compared to Reciproc, which could be due to the cross-sectional diameter [8, 10, 51–53]. Zhang et al. reported that the cross-sectional design influences the instruments’ mechanical properties. Further, the larger the cross-sectional area, the less flexible the file will be [54]. In addition to the metallurgical differences between

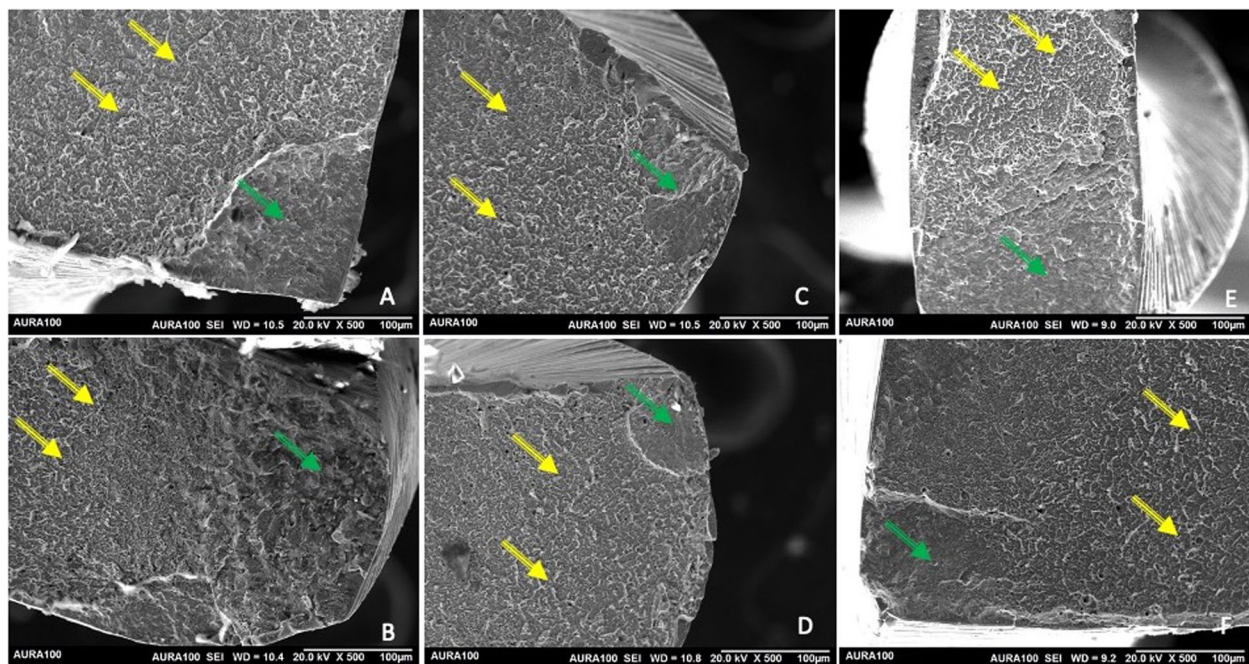


Fig. 5 Fractographic analysis images of ESR, RB, and WOG taken at 500X magnification using SEM. **A, C, and E** show fractured segments of ESR, RB, and WOV, respectively, after cyclic fatigue in static mode. **B, D, and F** show fractured segments of ESR, RB, and WOV, respectively, after fatigue in dynamic mode. Yellow arrows show areas of fatigue striations, and green arrows indicate a dimpled surface

these files, their cross-sectional shape may also influence their cyclic fatigue resistance. WaveOne Gold features a unique parallelogram-shaped cross-section, whereas both Reciproc Blue and Reciproc possess S-shaped cross-sections [55]. While there is no consensus on the impact of cross-sectional shape on cyclic fatigue resistance, several studies suggest that the dimensions of the cross-sectional area play a more critical role than the alloy type [8, 36]. Previous research has indicated that instruments with a larger metal core mass tend to have reduced fracture resistance [56]. Further investigation is needed to compare the cross-sectional areas of RB and WOG.

The DF mode groups exhibited a greater NCF than the SF mode groups. These results are consistent with previous studies [57, 58]. Hulsmann et al. reported that the DF mode has up to 150% greater fatigue resistance than the SF mode [59]. Further, the alloy phase transformation during the DF test prevents microcrack initiation, which also extends the instrument’s lifespan [39].

ESR, WOG, and RB were tested in the SF and DF modes using an artificial canal with a 60°-angle curvature. One of the drawbacks of laboratory studies is their lack of clinical relevance. It is challenging to assess the instruments’ fatigue behavior and mimic the clinical situation, given that instrument separation may be the combined result of torsional and cyclic stresses [60]. Several studies have used the SF and DF modes to evaluate cyclic fatigue

resistance [11, 53, 61, 62]. However, the DF test simulates the clinical situation [59]. Hence, we applied both modes to assess cyclic fatigue resistance. Extracted teeth are suitable specimens to assess these instruments’ cyclic fatigue. However, they are not standardized because of the differences in the length of the canal, degree, and radius of curvature, and dentin hardness. In this study, we choose to use an artificial canal rather than extracted teeth in our study to ensure standardization [63, 64].

In fatigue behavior studies, fractographic analysis identifies the fractured surface characteristics to determine the fracture mechanism [65]. In past decades, the longitudinal view was used to study the mode of fracture. More recently, the lateral view with magnifying loupes [65, 66] followed by an operating microscope [67, 68] has been adopted for fractographic examination. Satapan et al. used SEM to examine the features of instrument separation [28]. In fractographic analysis, striations characteristics could give an idea about the NCF. The presence of multiple crack initiation sites is known to extend the cyclic fatigue life of a material, as the applied stresses are distributed among the cracks. This reduces strain localization and slows the propagation of fatigue cracks [69]. Hence, a large striation area indicates slow crack propagation. By contrast, dimples in the center area indicate rapid crack propagation because of overload that exceeds the maximum level [70]. In this study crack

initiation was at the cutting edges [71, 72] with multiple crack origins suggesting a similar fracture mechanism.

Fractographic analysis of the fractured segments confirmed that the failure was attributable to cyclic fatigue in all groups. Moreover, we observed large striation areas in the DF mode groups compared to the SF mode groups. In the DF test, the files were subjected to back-and-forth axial movements that allowed stress to be distributed along with the instruments [49, 50]. This explains why the DF testing mode has a greater number of cycles, and a large striation area compared to the SF testing mode. Further studies are needed to investigate the DF resistance tests with various speed limits to explain the impact of speed on cyclic fatigue resistance.

Conclusions

Considering the limitation of the present in-vitro study, the following conclusions can be drawn; RB shows martensite transformation temperatures close to body temperature. ESR shows martensite transformation temperatures much lower than body temperature. Heat treatment of the evaluated files results in A_f temperature higher than working temperatures, which results in more stable martensite and R-phase. RB and ESR show better cyclic fatigue resistance compared to WOG. The results suggest using RB and ESR in curved and narrow canals.

Abbreviations

ESR	EndoSequence Reciprocating System
WOG	Wave One Gold
RB	Reciproc Blue
DSC	Differential Scanning Calorimetry
CCW	Counterclockwise
CW	Clockwise
M_s	Martensitic transformation-start temperature
M_f	Martensitic transformation-finish temperature
A_s	Austenitic transformation-start temperature
A_f	Austenitic transformation-finish temperature
NCF	Number of cycles to failure
SF	Static mode cyclic fatigue
DF	Dynamic mode cyclic fatigue
SEM	Scanning electron microscope

Supplementary Information

The online version contains supplementary material available at <https://doi.org/10.1186/s12903-025-05708-w>.

Supplementary Material 1.

Source of figures and permission to use them

All figures are the property of the authors, and they have permission to use them.

Authors' contributions

LA-Draft preparation, writing, review, and editing. MA-Formal analysis, methodology, and investigation. MA and MH-Writing, review, and editing. TA and SB-Data curation. RS-Resources. MH-Project administration and validation.

Funding

This research was funded by The Deanship of Scientific Research (DSR), King Abdulaziz University, Jeddah, Saudi Arabia, grant number G: 596–165-1441. The authors, therefore, acknowledge with thanks DSR for technical and financial support.

Data availability

The datasets used and/or analyzed during the current study are available from the corresponding author upon reasonable request. Data cannot be deposited in a public repository since this research is not yet published. For that reason, data confidentiality data will be granted upon reasonable request.

Declarations

Ethics approval and consent to participate

This study was approved by the Research Ethics Committee of the Faculty of Dentistry, King Abdulaziz University, proposal no. 195–12-20. Not Applicable.

Competing interests

The authors declare no competing interests.

Received: 26 September 2024 Accepted: 20 February 2025

Published online: 05 March 2025

References

- Miura F, Mogi M, Ohura Y, Hamanaka H. The super-elastic property of the Japanese NiTi alloy wire for use in orthodontics. *Am J Orthod Dentofacial Orthop.* 1986;90(1):1–10.
- Zhou HZ, Hu M, Yao J, Ma L. Rapid lengthening of rabbit mandibular ramus by using nitinol spring: a preliminary study. *J Craniofac Surg.* 2004;15(5):725–9.
- Khier SE, Brantley WA, Fournelle RA. Bending properties of superelastic and nonsuperelastic nickel-titanium orthodontic wires. *Am J Orthod Dentofacial Orthop.* 1991;99(4):310–8.
- Gluskin AH, Brown DC, Buchanan LS. A reconstructed computerized tomographic comparison of Ni-Ti rotary GT files versus traditional instruments in canals shaped by novice operators. *Int Endod J.* 2001;34(6):476–84.
- Generali L, Righi E, Todesca MV, Consolo U. Canal shaping with WaveOne reciprocating files: influence of operator experience on instrument breakage and canal preparation time. *Odontology.* 2014;102(2):217–22.
- Yared G. Canal preparation using only one Ni-Ti rotary instrument: preliminary observations. *Int Endod J.* 2008;41(4):339–44.
- De-Deus G, Moreira EJ, Lopes HP, Elias CN. Extended cyclic fatigue life of F2 ProTaper instruments used in reciprocating movement. *Int Endod J.* 2010;43(12):1063–8.
- Pedulla E, Grande NM, Plotino G, Gambarini G, Rapisarda E. Influence of continuous or reciprocating motion on cyclic fatigue resistance of 4 different nickel-titanium rotary instruments. *J Endod.* 2013;39(2):258–61.
- Ferreira F, Adeodato C, Barbosa I, Aboud L, Scelza P, Zaccaro Scelza M. Movement kinematics and cyclic fatigue of NiTi rotary instruments: a systematic review. *Int Endod J.* 2017;50(2):143–52.
- De-Deus G, Silva EJ, Vieira VT, Belladonna FG, Elias CN, Plotino G, Grande NM. Blue Thermomechanical Treatment Optimizes Fatigue Resistance and Flexibility of the Reciproc Files. *J Endod.* 2017;43(3):462–6.
- Gundogar M, Ozyurek T. Cyclic Fatigue Resistance of OneShape, HyFlex EDM, WaveOne Gold, and Reciproc Blue Nickel-titanium Instruments. *J Endod.* 2017;43(7):1192–6.
- Alghamdi A, Alsofi L, Balto K. Effects of a Novel NiTi Thermomechanical Treatment on the Geometric Features of the Prepared Root Canal System. *Materials (Basel)* 2020, 13(23).

13. Maki K, Ebihara A, Kimura S, Nishijo M, Tokita D, Miyara K, Okiji T. Enhanced root canal-centering ability and reduced screw-in force generation of reciprocating nickel-titanium instruments with a post-machining thermal treatment. *Dent Mater J*. 2020;39(2):251–5.
14. Van der Vyver P, Vorster M. WaveOne Gold Reciprocating Instruments in Clinical Practice (Part 1). *Endodontics Today*. 2021;18:32–5.
15. Fangli T, Maki K, Kimura S, Nishijo M, Tokita D, Ebihara A, Okiji T. Assessment of mechanical properties of WaveOne Gold Primary reciprocating instruments. *Dent Mater J*. 2019;38(3):490–5.
16. Brasseler U.S.A. Dental L: Brasseler USA ESR™ EndoSequence® Reciprocating File.
17. Kim J, Park JK, Kim HK, Unnithan AR, Kim CS, Park CH. Optimization of Electropolishing on NiTi Alloy Stents and Its Influence on Corrosion Behavior. *J Nanosci Nanotechnol*. 2017; 17(4):2333–9.
18. Agrawal PR, Chandak M, Nikhade PP, Patel AS, Bhopatkar JK. Revolutionizing endodontics: Advancements in nickel-titanium instrument surfaces. *J Conserv Dent Endod*. 2024;27(2):126–33.
19. Huang X, Ackland GJ, Rabe KM. Crystal structures and shape-memory behaviour of NiTi. *Nat Mater*. 2003;2(5):307–11.
20. Daly S, Ravichandran G, Bhattacharya K. Stress-induced martensitic phase transformation in thin sheets of Nitinol. *Acta Mater*. 2007;55:3593–600.
21. Perez F, Schoumacher M, Peli JF. Shaping ability of two rotary instruments in simulated canals: stainless steel ENDOflash and nickel-titanium HERO Shaper. *Int Endod J*. 2005;38(9):637–44.
22. Yahata Y, Yoneyama T, Hayashi Y, Ebihara A, Doi H, Hanawa T, Suda H: Effect of heat treatment on transformation temperatures and bending properties of nickel-titanium endodontic instruments. *Int Endod J* 2009, 42(7):621–626.
23. Alsofi L, Rajkhan W, Al-Habib M, Ashe H, Alnowailaty Y, Balto K. Characterization of the differential efficacy of austenitic vs martensitic NiTi rotary files in non-surgical root canal retreatment: a micro-CT analysis. *Front Biosci (Landmark Ed)*. 2021;26(9):465–74.
24. Bradley TG, Brantley WA, Culbertson BM. Differential scanning calorimetry (DSC) analyses of superelastic and nonsuperelastic nickel-titanium orthodontic wires. *Am J Orthod Dentofacial Orthop*. 1996;109(6):589–97.
25. Brantley WA, Svec TA, Iijima M, Powers JM, Grentzer TH. Differential scanning calorimetric studies of nickel titanium rotary endodontic instruments. *J Endod*. 2002;28(8):567–72.
26. Parashos P, Gordon I, Messer HH. Factors influencing defects of rotary nickel-titanium endodontic instruments after clinical use. *J Endod*. 2004;30(10):722–5.
27. Parashos P, Messer HH. Rotary NiTi instrument fracture and its consequences. *J Endod*. 2006;32(11):1031–43.
28. Sattapan B, Nervo GJ, Palamara JE, Messer HH. Defects in rotary nickel-titanium files after clinical use. *J Endod*. 2000;26(3):161–5.
29. Ullmann CJ, Peters OA. Effect of cyclic fatigue on static fracture loads in ProTaper nickel-titanium rotary instruments. *J Endod*. 2005;31(3):183–6.
30. Cheung GS, Peng B, Bian Z, Shen Y, Darvell BW. Defects in ProTaper S1 instruments after clinical use: fractographic examination. *Int Endod J*. 2005;38(11):802–9.
31. Kasuga Y, Kimura S, Maki K, Unno H, Omori S, Hirano K, Ebihara A, Okiji T. Phase transformation and mechanical properties of heat-treated nickel-titanium rotary endodontic instruments at room and body temperatures. *BMC Oral Health*. 2023;23(1):825.
32. Miyai K, Ebihara A, Hayashi Y, Doi H, Suda H, Yoneyama T: Influence of phase transformation on the torsional and bending properties of nickel-titanium rotary endodontic instruments. *Int Endod J* 2006, 39(2):119–126.
33. Hou X, Yahata Y, Hayashi Y, Ebihara A, Hanawa T, Suda H. Phase transformation behaviour and bending property of twisted nickel-titanium endodontic instruments. *Int Endod J*. 2011;44(3):253–8.
34. Pedulla E, Lo Savio F, Boninelli S, Plotino G, Grande NM, La Rosa G, Rapisarda E. Torsional and Cyclic Fatigue Resistance of a New Nickel-Titanium Instrument Manufactured by Electrical Discharge Machining. *J Endod*. 2016;42(1):156–9.
35. Adiguzel M, Capar ID. Comparison of Cyclic Fatigue Resistance of WaveOne and WaveOne Gold Small, Primary, and Large Instruments. *J Endod*. 2017;43(4):623–7.
36. Pruett JP, Clement DJ, Carnes DL Jr. Cyclic fatigue testing of nickel-titanium endodontic instruments. *J Endod*. 1997;23(2):77–85.
37. Nguyen HH, Fong H, Paranjpe A, Flake NM, Johnson JD, Peters OA. Evaluation of the resistance to cyclic fatigue among ProTaper Next, ProTaper Universal, and Vortex Blue rotary instruments. *J Endod*. 2014;40(8):1190–3.
38. Shen Y, Zhou HM, Zheng YF, Peng B, Haapasalo M. Current challenges and concepts of the thermomechanical treatment of nickel-titanium instruments. *J Endod*. 2013;39(2):163–72.
39. Zupanc J, Vahdat-Pajouh N, Schafer E. New thermomechanically treated NiTi alloys - a review. *Int Endod J*. 2018;51(10):1088–103.
40. Alsofi L, Al Harbi M, Stauber M, Balto K: Analysis of the Morpho-Geometrical Changes of the Root Canal System Produced by TF Adaptive vs. BioRace: A Micro-Computed Tomography Study. *Materials (Basel)* 2021, 14(3).
41. Hieawy A, Haapasalo M, Zhou H, Wang ZJ, Shen Y. Phase Transformation Behavior and Resistance to Bending and Cyclic Fatigue of ProTaper Gold and ProTaper Universal Instruments. *J Endod*. 2015;41(7):1134–8.
42. Shen Y, Zhou H, Coil JM, Aljazeera B, Buttari R, Wang Z, Zheng YF, Haapasalo M. ProFile Vortex and Vortex Blue Nickel-Titanium Rotary Instruments after Clinical Use. *J Endod*. 2015;41(6):937–42.
43. Otsuka K, Ren X. Physical metallurgy of Ti–Ni-based shape memory alloys. *Prog Mater Sci*. 2005;50(5):511–678.
44. Hosseini SA, Sadrnezhad SK, Ekrami A. Phase transformation behavior of porous NiTi alloy fabricated by powder metallurgical method. *Mater Sci Eng, C*. 2009;29(7):2203–7.
45. Wang X, Verlinden B, Humbeeck J. R-phase transformation in NiTi alloys. *Mater Sci Technol*. 2014;30:1517–29.
46. Tsujimoto M, Irifune Y, Tsujimoto Y, Yamada S, Watanabe I, Hayashi Y. Comparison of Conventional and New-generation Nickel-Titanium Files in Regard to Their Physical Properties. *Journal of Endodontics*. 2014;40(11):1824–9.
47. Alapati SB, Brantley WA, Iijima M, Clark WAT, Kovarik L, Buie C, Liu J, Ben Johnson W. Metallurgical Characterization of a New Nickel-Titanium Wire for Rotary Endodontic Instruments. *Journal of Endodontics*. 2009;35(11):1589–93.
48. Shen Y, Zhou H-m, Zheng Y-f, Campbell L, Peng B, Haapasalo M: Metallurgical Characterization of Controlled Memory Wire Nickel-Titanium Rotary Instruments. *J Endodont*. 2011;37(11):1566–71.
49. Lopes HP, Elias CN, Vieira MV, Siqueira JF Jr, Mangelli M, Lopes WS, Vieira VT, Alves FR, Oliveira JC, Soares TG. Fatigue Life of Reciproc and Mtwo instruments subjected to static and dynamic tests. *J Endod*. 2013;39(5):693–6.
50. Pedulla E, Lizio A, Scibilia M, Grande NM, Plotino G, Boninelli S, Rapisarda E, Lo Giudice G. Cyclic fatigue resistance of two nickel-titanium rotary instruments in interrupted rotation. *Int Endod J*. 2017;50(2):194–201.
51. Plotino G, Grande NM, Testarelli L, Gambarini G. Cyclic fatigue of Reciproc and WaveOne reciprocating instruments. *Int Endod J*. 2012;45(7):614–8.
52. Alcalde MP, Duarte MAH, Bramante CM, de Vasconcelos BC, Tanomaru-Filho M, Guerreiro-Tanomaru JM, Pinto JC, So MVR, Vivian RR. Correction to: Cyclic fatigue and torsional strength of three different thermally treated reciprocating nickel-titanium instruments. *Clin Oral Investig*. 2018;22(4):1879.
53. Keskin C, Inan U, Demiral M, Keles A. Cyclic Fatigue Resistance of Reciproc Blue, Reciproc, and WaveOne Gold Reciprocating Instruments. *J Endod*. 2017;43(8):1360–3.
54. Zhang EW, Cheung GS, Zheng YF. Influence of cross-sectional design and dimension on mechanical behavior of nickel-titanium instruments under torsion and bending: a numerical analysis. *J Endod*. 2010;36(8):1394–8.
55. Topcuoglu HS, Duzgun S, Akti A, Topcuoglu G. Laboratory comparison of cyclic fatigue resistance of WaveOne Gold, Reciproc and WaveOne files in canals with a double curvature. *Int Endod J*. 2017;50(7):713–7.
56. Kim HC, Kwak SW, Cheung GS, Ko DH, Chung SM, Lee W. Cyclic fatigue and torsional resistance of two new nickel-titanium instruments used in reciprocation motion: Reciproc versus WaveOne. *J Endod*. 2012;38(4):541–4.
57. Li UM, Lee BS, Shih CT, Lan WH, Lin CP. Cyclic fatigue of endodontic nickel titanium rotary instruments: static and dynamic tests. *J Endod*. 2002;28(6):448–51.
58. Rodrigues RC, Lopes HP, Elias CN, Amaral G, Vieira VT, De Martin AS. Influence of different manufacturing methods on the cyclic fatigue of rotary nickel-titanium endodontic instruments. *J Endod*. 2011;37(11):1553–7.

59. Hulsman M, Donnermeyer D, Schafer E. A critical appraisal of studies on cyclic fatigue resistance of engine-driven endodontic instruments. *Int Endod J*. 2019;52(10):1427–45.
60. Plotino G, Grande NM, Cordaro M, Testarelli L, Gambarini G. A review of cyclic fatigue testing of nickel-titanium rotary instruments. *J Endod*. 2009;35(11):1469–76.
61. Elnaghy AM, Elsaka SE. Effect of sodium hypochlorite and saline on cyclic fatigue resistance of WaveOne Gold and Reciproc reciprocating instruments. *Int Endod J*. 2017;50(10):991–8.
62. Ozyurek T. Cyclic Fatigue Resistance of Reciproc, WaveOne, and WaveOne Gold Nickel-Titanium Instruments. *J Endod*. 2016;42(10):1536–9.
63. Yao JH, Schwartz SA, Beeson TJ. Cyclic fatigue of three types of rotary nickel-titanium files in a dynamic model. *J Endod*. 2006;32(1):55–7.
64. Ajuz NC, Armada L, Goncalves LS, Debelian G, Siqueira JF Jr. Glide path preparation in S-shaped canals with rotary pathfinding nickel-titanium instruments. *J Endod*. 2013;39(4):534–7.
65. Gabel WP, Hoen M, Steiman HR, Pink FE, Dietz R. Effect of rotational speed on nickel-titanium file distortion. *J Endod*. 1999;25(11):752–4.
66. Daugherty DW, Gound TG, Comer TL. Comparison of fracture rate, deformation rate, and efficiency between rotary endodontic instruments driven at 150 rpm and 350 rpm. *J Endod*. 2001;27(2):93–5.
67. Tygesen YA, Steiman HR, Ciavarrro C. Comparison of distortion and separation utilizing profile and Pow-R nickel-titanium rotary files. *J Endod*. 2001;27(12):762–4.
68. Arens FC, Hoen MM, Steiman HR, Dietz GC Jr. Evaluation of single-use rotary nickel-titanium instruments. *J Endod*. 2003;29(10):664–6.
69. Pirani C, Ruggeri O, Cirulli PP, Pelliccioni GA, Gandolfi MG, Prati C. Metallurgical analysis and fatigue resistance of WaveOne and ProTaper nickel-titanium instruments. *Odontology*. 2014;102(2):211–6.
70. Pirani C, Iacono F, Generali L, Sassatelli P, Nucci C, Lusvarghi L, Gandolfi MG, Prati C. HyFlex EDM: superficial features, metallurgical analysis and fatigue resistance of innovative electro discharge machined NiTi rotary instruments. *Int Endod J*. 2016;49(5):483–93.
71. Cheung GS, Darvell BW: Fatigue testing of a NiTi rotary instrument. Part 2: Fractographic analysis. *Int Endod J* 2007, 40(8):619–625.
72. Shen Y, Qian W, Abtin H, Gao Y, Haapasalo M. Fatigue testing of controlled memory wire nickel-titanium rotary instruments. *J Endod*. 2011;37(7):997–1001.

Publisher's Note

Springer Nature remains neutral with regard to jurisdictional claims in published maps and institutional affiliations.